Modelling Reflex Recruitment of Neck Muscles in a Finite Element Human Body Model for Simulating Omnidirectional Head Kinematics

Jóna M. Ólafsdóttir, Jonas Östh, Karin Brolin

Abstract Numerical human body models that can predict occupant head and neck responses are essential for the development and assessment of motor vehicle safety systems. Including the contribution of neck muscle responses is needed to improve model predictions, in particular during simulated pre-crash manoeuvers. While a general purpose model that can predict head-neck kinematics in various pre-crash conditions (e.g. emergency braking and steering) is needed most current models have been limited to predictions of longitudinal motion (e.g. during emergency braking). We developed a method for simulating muscle recruitment in a finite element human body model for omnidirectional head-neck kinematics predictions. A neural control scheme that uses kinematics and muscle length feedback to determine the activation level in individual muscle elements was implemented. The control scheme included a novel approach to determine load sharing between muscles based on experimental data from human subjects in dynamic conditions. Multidirectional 1 g loading conditions were simulated to assess the effect of muscle recruitment on head and neck kinematics in multiple directions and to evaluate the predicted spatial tuning of recruitment for selected muscles. Simulation results demonstrate that including both kinematics and muscle length feedback reduces head and internal neck motion induced from external 1 g loading.

Keywords Active muscle, feedback, head kinematics, human body model, neck kinematics.

I. INTRODUCTION

Detailed numerical models of the human body are increasingly used by researchers and the automotive industry for the development of safety systems. For example, human body models (HBMs) can be used to predict occupant head and neck kinematics preceding and during crashes to study the influence of advanced seatbelt designs on the occupant response [1,2]. Studies indicate that occupant dynamics during vehicle pre-crash manoeuvers may influence occupant crash kinematics [3–5]. To improve crash kinematics predictions, HBMs should simulate occupant postural responses and the associated muscle recruitment strategies during vehicle manoeuvers, such as emergency braking and steering, which may proceed the crash.

Muscle recruitment is complex and specific kinematics can be achieved with different muscle recruitment strategies. Various methodologies for simulating neck muscle recruitment in HBMs for crash simulations have therefore been proposed in the past. Several models introduced the effect of reflex muscle responses by applying maximum or close to maximum activity at a pre-defined time in the simulation [6–11]. Although this approach may be representative of responses during short duration impacts, it is less applicable for simulating posture maintenance during pre-crash manoeuvers. Other models used optimization to determine muscle activity during impacts [3,12–14]. However, as pointed out in [15] the objective functions used (such as minimizing energy, muscle forces, stiffness or total work) may not be relevant to impact scenarios and that muscle recruitment in cases where efficiency is not the main objective has not been adequately explored. Muscle recruitment determined from normalized electromyogram (EMG) measured in volunteer experiments has been used in whole body HBMs and lower extremity models [16–20]. A major drawback of using EMG to prescribe muscle activity is the need for collecting volunteer data for each new load scenario of interest. Methods with pre-defined muscle activity are case specific and thus have limited applicability for the development of safety systems as occupant interaction with new restraint systems is likely to change muscle activity.

Recent models have proposed closed-loop control where muscle activation is regulated based on sensory

J. M. Ólafsdóttir (jona.olafsdottir@chalmers.se) and J. Östh were Researchers and K. Brolin is a Professor at the Department of Mechanics and Maritime Sciences at Chalmers University of Technology, Gothenburg, Sweden.

information about the current state of the model to better represent the feedback mechanisms of the central nervous system (CNS) [2,21–29]. The benefit of including physiological feedback loops in neural control schemes in HBMs is the potential ability to predict responses in a wide range of pre-crash scenarios as the level of muscle activation can be continuously adjusted based on changes in the external environment (e.g. magnitude and direction of acceleration). Closed loop control was first implemented with multi body HBMs using Proportional-Integral-Derivative (PID) controllers that applied torques to regulate the joint angle at each individual vertebral joint [21,22,29]. Subsequently, multi body and finite element models with muscle elements have implemented PID controllers that use head kinematics feedback to regulate neck muscle activity in simulations of pre-crash scenarios [2,21–26,28]. Head kinematics based closed-loop control emulates vestibular feedback of the CNS but omits contribution from muscle spindle feedback. Control with only head kinematics feedback does therefor not consider internal neck kinematics which may result in non-physiological vertebral movement. Simulations have shown that during small oscillations, while head kinematics feedback was a major contributor to stabilising the head and neck, incorporating muscle length (spindle) feedback was necessary to stabilise individual neck joints and prevent neck buckling, indicating the importance of including both feedback loops [28]. Combined kinematics and muscle length feedback and the influence of muscle length feedback on neck kinematics has not been well studied in loading conditions that generate head displacements of similar magnitude to what can be expected during pre-crash manoeuvers.

Most current HBMs that simulate pre-crash occupant kinematics have been applied in longitudinal conditions, where anterior-posterior movement was induced [2,21–25,27]. For HBMs to predict occupant head movement in a wide range of pre-crash scenarios models must be able to respond to excitation in multiple directions. A major challenge in simulating omnidirectional head movement is presented by the uncertainty of how load is shared between more than 25 neck muscle pairs. How the CNS in humans determines the relative contribution of individual neck muscles during dynamic conditions from external perturbation has not been adequately explored and experimental data is scarce. Consequently, no HBMs that can simulate and predict omnidirectional pre-crash head kinematics are currently available.

In this study, we implemented a neural control scheme for regulating neck muscle activity in a finite element HBM. The proposed scheme included head kinematics and muscle length feedback with muscle load sharing definition based on in vivo data on neck muscle recruitment patterns from a dynamic sled experiment [30]. We studied the model's capability to counteract induced motion from inertial loading in multiple directions and the spatial tuning of muscle recruitment. The objective of this study was to explore how the different feedback loops in the neural control scheme influenced head-neck kinematics and muscle recruitment. This insight may help guide future modelling efforts and collection of experimental data for model validation.

II. METHODS

A 50th percentile male, whole-body finite element HBM (Fig. 1A) was used in this study. It was a modified version of the Total Human Model for Safety (THUMS) version 3.0 (Toyota Central R&D Labs., Inc., Nagakute, Aichi, Japan) published in Östh et al. [25]. The skin material properties were modified according to a recent model developed for low-g simulations [31]. The extremities were omitted to reduce computational time. All pre-defined muscle elements were removed and 188 one-dimensional Hill-type elements were added to represent the 28 neck muscle pairs listed in Table I (detailed description in Table AI in the Appendix). The activation levels of individual muscle elements were determined by the neural control scheme described below. All simulations were performed with the finite element solver LS-DYNA MPP v971 R8.0.0 (LSTC, Livermore, CA) using standard keywords.

Reflex recruitment model

The reflex recruitment model consisted of a closed-loop system of the head-neck complex with neural control that generates muscle activity in the Hill elements (Fig. 2). The neural control consisted of two reflex loops, representing neural feedback from the vestibular system and muscle spindles. The vestibular control loop uses kinematics based feedback and recruits pre-defined groups of muscles to maintain head posture, while the muscle spindle loops regulate individual muscle element lengths. The kinematics feedback consisted of sensory

information about the net angular deviation, θ, of the head-neck vector (defined as the vector from T1 vertebral body geometrical centre to head centre of gravity (CG)) from initial position (see Fig. 3) and the corresponding angular speed, $\dot{\theta}$, referred to as kinematics feedback (KF). Kinematics feedback was multiplied by constant gains, k_θ and $k_{\dot{\theta}}$, adopted from an earlier study with the current HBM [2]. These gains were obtained by tuning using optimization methods to one set of volunteer tests and validated with respect to another set of test data [2].

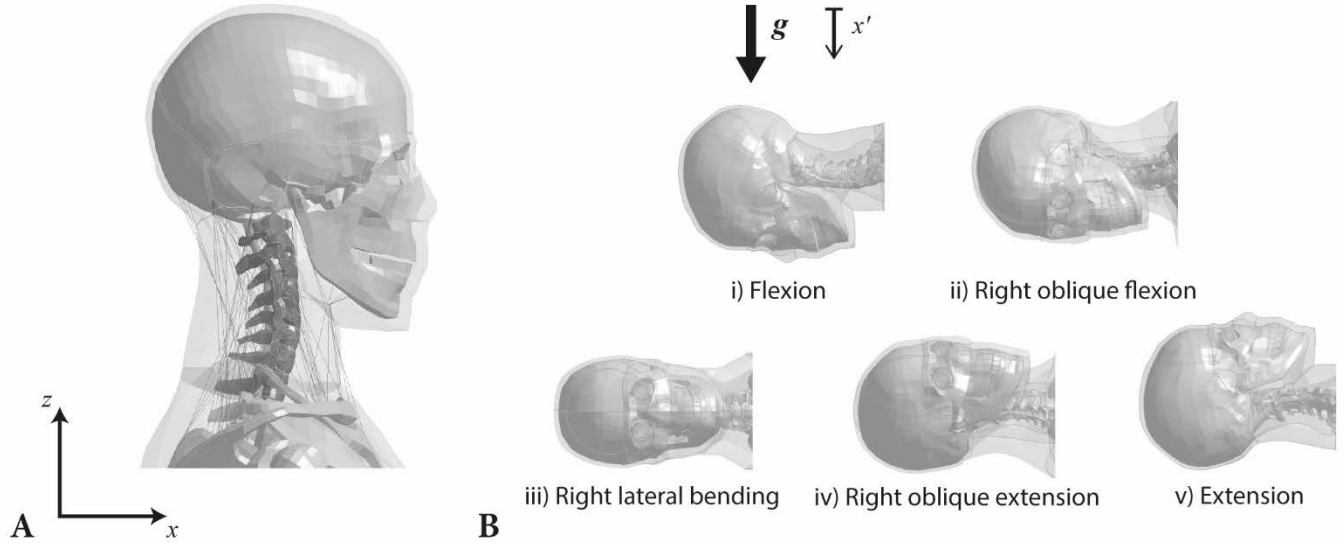

Fig. 1. A) The THUMS finite element model depicted here in the global coordinate system. B) Illustration of the model's initial position in the multidirectional response simulations for all five conditions i)-iv) in different views, such that direction of the gravity field and the local *x*-axis, *x*′, are aligned in the figure.

TABLE I
MUSCLES REPRESENTED IN THE MODEL (SINGLE SIDE), NUMBER OF LINE ELEMENTS PER MUSCLE, AND THE RESPECTIVE EXPERMENTAL EMG SPATIAL TUNING PATTERN ASSIGNED TO EACH MUSCLE.

Muscle	Nr. of elem.	Assigned pattern*	Muscle	Nr. of elem.	Assigned pattern*
Sternocleidomastoid (SCM)	2		Semispinalis capitis (SCap)	5	
Scalenus posterior	3		Rectus capitis posterior minor	1	SCap
Scalenus medius	6	SCM	Rectus capitis posterior major	1	
Scalenus anterior	4		Obliqus capitis superior	1	
Rectus capitis anterior	1		Semispinalis cervicis (Scerv)	4	
Sternohyoid (STH)	2		Semispinalis thoracis	2	
Sternothyroid	2		Splenius capitis**	6	
Omohyoid	1		Splenius cervicis	3	Scerv
Longus colli superior oblique	3	STH	Erector spinae longissimus catpitis	8	
Longus colli vertical	4		Erector spinae longissimus cervicis	5	
Longus colli inferior oblique	2		Erector spinae iliocostalis cervicis	3	
Longus capitis	4		Multifidus cervicis (CM-C4)	3	CM-C4
Levator scapulae (LS)	4	LS	Multifidus cervicis (CM-C6)	9	
Trapezius (Trap)	3	Trap	Obliqus capitis inferior	1	CM-C6
			Rectus capitis lateralis	1	

*The assigned patterns define the direction and muscle specific weights, w_i, in Equation (1). The assigned experimental tuning patterns from [30] are shown in Fig. A1 in the Appendix.

**Splenius capitis was assigned the same pattern as semispinalis cervicis due to ambiguity in the experimental findings for this muscle.

The KF loop generates a single control signal, referred to as the excitation signal, u_K. To define the load sharing between the multiple neck muscles, that is, the relative contributions of each muscle in response to the excitation signal, u_K, the 28 muscle pairs were split into 16 groups (eight on each side) and a weighting function, $w_i(\alpha)$, defined for each group i. The variable α varies with head motion and is the angle of the projection of the head-neck vector in the horizontal plane (see Fig. 3). The muscle group specific excitation signal, $u_{K,i}$, which defines the relative excitation of each muscle group was then obtained by

$$u_{K,i} = w_i(\alpha)u_K \quad (1)$$

where $i = 1, \dots, 16$ denoting the number of muscle groups. The angle α varies over time and was updated in every time step during simulation. Fig. 3 shows a schematic of the angle α and illustrates how the weights of each muscle group, w_i, were determined based on α and experimentally derived EMG spatial tuning patterns from dynamic sled tests [30]. In the experiment seated volunteers were exposed to 1.55 g perturbations in eight directions (0°, ±45°, ±90°, ±135°, 180°) and EMG in eight left neck muscles was measured with intramuscular electrodes. The corresponding muscles in the head-neck model were assigned the respective experimental patterns, normalised by the highest amplitude for any muscle (0.886 for semispinalis capitis, Fig. A1), see Table I. The remaining modelled muscles, for which no experimental data was available, were grouped with and assigned the pattern of a muscle of similar anatomical function (Table I). The muscles with the same assigned pattern act synergistically and are recruited as a group in response to a positive u_K signal. A total of $i = 16$ muscle groups, eight on each side, to each a unique experimental pattern was assigned was achieved by assuming symmetry between left and right side muscle responses and mirroring the experimental patterns around the 0° - 180° axis to generate patterns for right sided muscles (Fig. A1). Signal transmission and neural processing times were expressed as a time delay, T_K = 20 ms (estimated based on [32]).

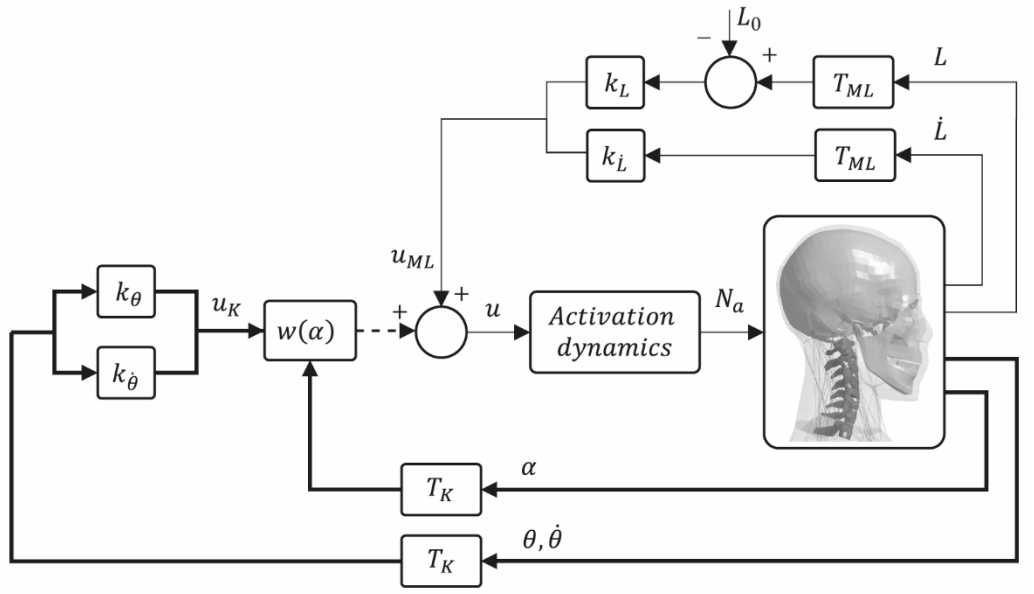

Fig. 2. Schematic illustration of the neural control scheme for regulating reflex neck muscle activity based on both kinematics and muscle length feedback. Thick arrows represent a single signal, dotted arrow group specific signals (no. = 16) and thin arrows muscle specific signals (no. = 188).

Muscle length feedback (MLF) was implemented for each muscle element by sensing its absolute length, L, and lengthening velocity, $\dot{L}$. The excitation signal, $u_{ML,j}$, was generated if the current length exceeded the reference length, L_0, representing the element's length at loading onset. MLF was only triggered during dynamic loading. Muscle length feedback was multiplied with constant gains, k_L and $k_{\dot{L}}$, where $k_{\dot{L}}/k_L = 0.1$ [33]. Equal gains were used for each muscle element. Neural transmission and processing time was assumed as a time delay of T_{ML} = 10 ms (estimated based on [34]).

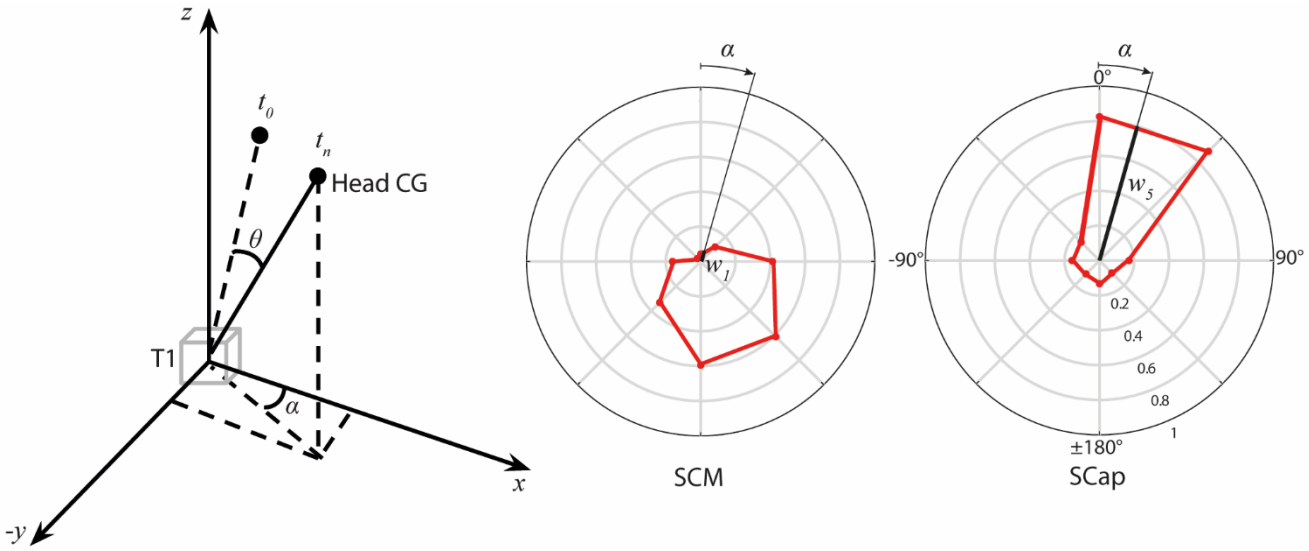

Fig. 3. The schematic shows how head-neck vector (head CG to T1) angle, θ, was defined and how α was determined using the head-neck vector projection in the horizontal plane for an arbitrary point in time, t_n, (time zero denoted t_0) exemplified for right oblique flexion of the head-neck. The polar plots show how the weights, w_i, were determined for a given α for two exemplar muscles, left sternocleidomastoid (SCM) and semispinalis capitis (SCap). The red curves are the experimental spatial tuning curves for SCM and SCap from [30], also shown in Fig. A1 in the Appendix.

When both KF and MLF were included (referred to as KMLF), the excitation signal of each muscle element assumed a linear combination of the respective KF and MLF signals

$$u_j = u_{K,i} + u_{ML,j} \tag{2}$$

where $j = 1, \ldots, 188$ denotes the total number of muscle elements. The u_j therefore represents an excitation signal specific to every muscle element. Muscle activation dynamics from excitation signal, u_j, to activation level, $N_{a,j}$, were modelled as a set of two first order differential equations as described by [35]

$$\frac{dN_{e,j}}{dt} = \frac{\left(u_j - N_{e,j}\right)}{T_{ne}} \tag{3}$$

$$\frac{dN_{a,j}}{dt} = \begin{cases} \dfrac{\left(N_{e,j} - N_{a,j}\right)}{T_{na,a}}, & N_{e,j} \geq N_{a,j} \\ \dfrac{\left(N_{e,j} - N_{a,j}\right)}{T_{na,d}}, & N_{e,j} < N_{a,j} \end{cases} \tag{4}$$

The first system, Equation (3), represents excitation dynamics where $N_{e,j}$ denotes an intermediate neural excitation level. The second system, Equation (4), represents the contraction dynamics of the muscle. The two conditions in Equation (4) represent activation and deactivation where the time constant for deactivation, $T_{na,d}$, is larger than for activation, $T_{na,a}$. The time constants, $T_{x,y}$, and other control parameters are summarised in Table II. Activation levels were constrained between a predefined minimum contraction level, $0.05w_i$, and maximum contraction of one. The minimum contraction level was chosen based on the highest average neck EMG recorded in volunteers during quiet sitting while riding as passengers in a car, 4.7±4.1 %MVC (percent of maximum voluntary contraction), reported in [36].

TABLE II
SUMMARY OF FEEDBACK GAINS, TIME DELAYS, AND TIME CONSTANTS.

KF gains	k_θ	1.3	
	$k_{\dot{\theta}}$	470	
MLF gains	k_L	0.5	
	$k_{\dot{L}}$	0.05	
Time delays	T_K	20 ms	[32]
	T_{ML}	10 ms	[34]
Time constants	T_{ne}	35 ms	
	$T_{na,a}$	10 ms	
	$T_{na,d}$	40 ms	

Multidirectional response and spatial tuning verification

To explore the capability of the proposed neural control scheme to generate muscle recruitment patterns and to verify the spatial tuning of recruitment, simulations were performed where inertial head motion was induced in various directions. In physical terms, the simulations replicated a setup where a subject would be lying and the head support rapidly removed without warning. The HBM was exposed to instantaneously applied gravity loading in five simulations, varying the direction of the loading in the transverse plane at intervals of 45°, see Fig. 1B. The applied load in each of these five conditions resulted in neck: i) flexion, ii) right oblique flexion, iii) right lateral bending, iv) right oblique extension, and v) extension. The minimum contraction level was reduced to $0.03w_i$ based on the assumption that neck muscle activity is likely lower while lying with the head supported compared to upright posture with unsupported head. The HBM was constrained in space below the T3 vertebra throughout the duration of the simulation in all conditions.

To study the effect of each reflex loop on the model response, the five conditions were simulated with KMLF, only KF, and only MLF. This was compared to the passive model response without muscle activation ($u_j = 0$). An additional simulation was run to test the ability of the neural control to stabilise the head in an upright posture against gravity for 2 s. The minimum contraction level was $0.05w_i$ in this simulation. As MLF triggers during dynamic loading this simulation with KMLF is effectively KF only. Model kinematics were assessed by comparing simulated head CG translational displacements and peak rotations as well as selected vertebral rotations when applying KMLF, KF, and MLF. Model head displacements are reported in local coordinate systems which share an origin with the global coordinate system but are rotated so that the new *x*-axis, *x'*, is aligned with the direction of loading (Fig. 1B). Additional simulations were run to verify the isometric strength of the muscles. These results are reported in the Appendix.

The spatial tuning of muscle recruitment generated by KF was verified by comparing the simulated responses to the implemented experimental tuning patterns from [30]. The influence of MLF on spatial tuning was explored by comparing the tuning curves of the three neural control schemes, KF, MLF, and KMLF. Tuning curves were constructed by extracting the muscle activation level of the elements representing eight left sided muscles (SCM, STH, LS, Trap, SCap, SCerv, CM-C4 and CM-C6, see Table I) at 110 ms after loading onset in each loading direction. Based on model symmetry, activation levels of these left sided muscles in left oblique flexion, left lateral bending, and left oblique extension was assumed to be equal to the corresponding right sided muscle activity in the ii)-iv) conditions.

III. RESULTS

Neural control with KMLF reduced head displacement in all loading directions compared to the passive HBM, Fig. 4. Peak displacements were generally larger with KF or MLF only (12 – 20 mm and 0 – 9 mm larger, respectively). For instance, during induced flexion (0° loading direction in Figs. 4 and 5) peak displacement was 46 mm with KMLF, compared to 58 mm and 51 mm with KF and MLF, respectively. MLF reduced head displacement more than KF and for 45° and 90° loading directions MLF resulted in peak displacement equal to KMLF, 46 mm and 57 mm, respectively. Simulation of upright posture in gravity resulted in a stable posture with a net 7 mm rearward head CG displacement and 0.3° Y-rotation (flexion).

The spatial tuning of muscle recruitment with KF were verified and are shown in Fig. A1 in the Appendix. The resulting spatial tuning patterns with KMLF, KF, and MLF are illustrated in Fig. 5. Including muscle length feedback,

the KMLF resulted in similarly shaped spatial tuning patterns, except for STH and Trap. Muscle length feedback increased muscle activity mainly in the direction of preferred activation (0° and -45° for SCM, -135° and 180° for others), excluding SCap. Large differences in spatial tuning were found for the STH. Recruiting muscles solely based on element length (MLF) resulted in similar spatial patterns as with KMLF (excluding SCap) but of lower amplitudes. Co-contraction, the muscle activity during head movement where the respective muscle acts as an antagonist, was generally lower with MLF because muscles did not lengthen when acting as antagonists.

MLF resulted in substantially higher peak head rotations compared to KF and KMLF during induced flexion (20° vs. 8° and 11°, respectively) and right oblique flexion (14° vs. 6° and 9° Y-rotation, respectively, see Table 3). However, MLF generally resulted in less rotation of the C7, C4, and C2 vertebra in all loading directions. KMLF therefore had a combined effect with smaller vertebral rotations than KF (up to 12° less C4 Y-rotation) and smaller head rotation than MLF (up to 9° less Y-rotation) in all directions. KMLF, KF, and MLF had similar axial rotations for the head and vertebrae in all loading directions. Fig. 6 shows a visual comparison of the model response at 200 ms for two load cases, 0° and 90°, illustrating the effect of MLF and KF on spinal curvature and head rotation.

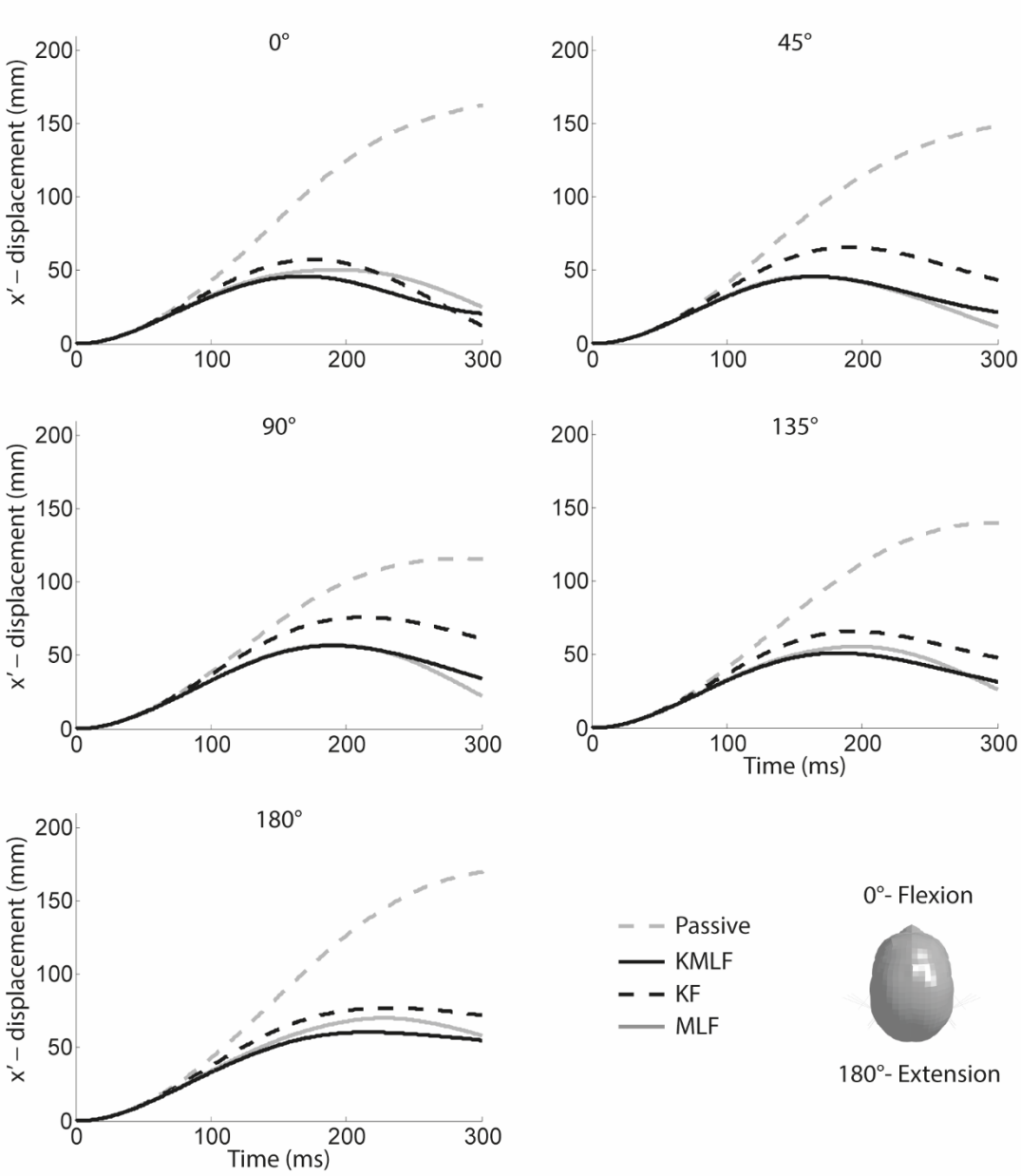

Fig. 4. Head CG displacement in a local coordinate system with the *x′*-axis along the direction of loading, for the passive model (grey dashed line) and with neural feedback: KMLF (black solid line), KF (black dashed line) and MLF (grey solid line).

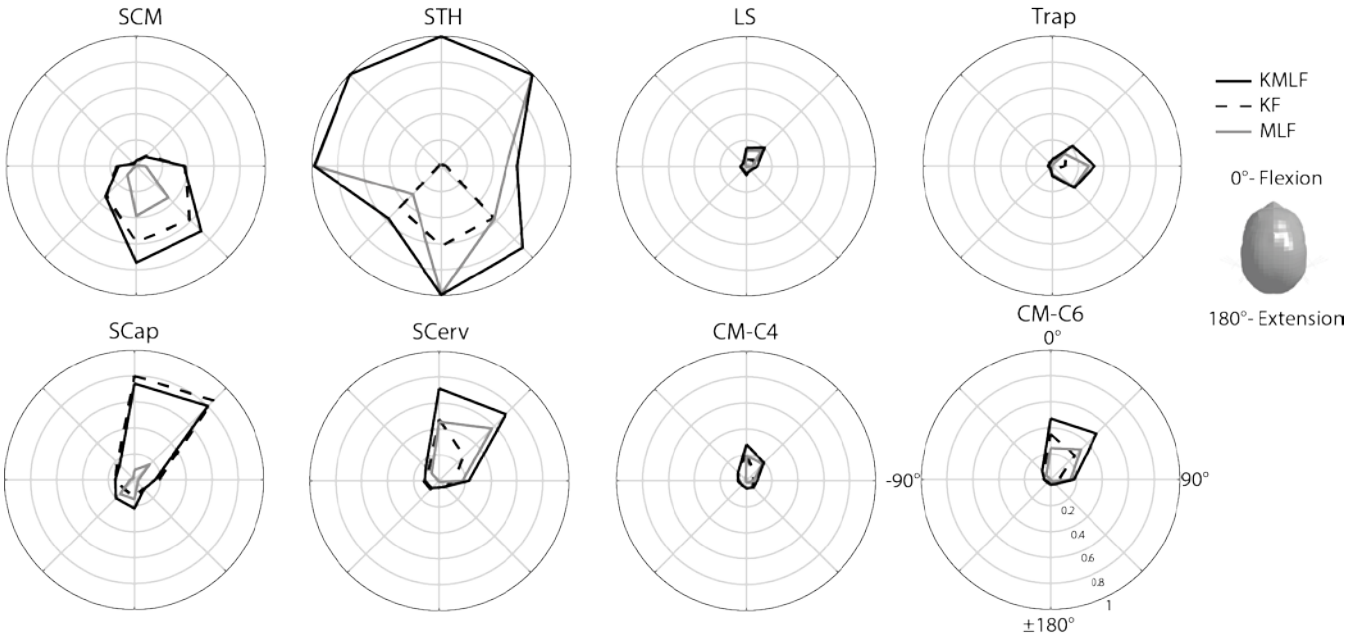

Fig. 5. Spatial tuning curves showing left muscle activation levels at 110 ms after loading onset generated by the neural control scheme (KMLF) and the separate KF and MLF loops. The '1' on the perimeter represents 100% activity.

TABLE III
AMPLITUDE (°) AND TIMING (MS) OF PEAK HEAD ROTATIONS AND CORRESPONDING ROTATIONS OF C7, C4, AND C2 VERTEBRA FOR KMLF, KF, AND MLF DURING MULTIDIRECTIONAL LOADING (R. RIGHT). ALL ROTATIONS ARE REPORTED IN THE GLOBAL COORDINATE SYSTEM (FIG. 1A).

Neural		*Flexion (0°)*					*R. oblique flex (45°)*			
control	*t* (ms)	**C7**	**C4**	**C2**	**H**	*t* (ms)	**C7**	**C4**	**C2**	**H**
X-rot										
KMLF			<±1			154	3	9	10	7
KF			<±1			175	5	14	17	7
MLF			<±1			176	3	9	9	8
Y-rot										
KMLF	154	7	13	15	11	173	6	10	10	9
KF	155	9	20	23	8	179	8	21	24	6
MLF	178	7	12	11	20	180	6	7	5	14
Z-rot										
KMLF			<±1			162	-3	-7	-8	-10
KF			<±1			180	-2	-7	-7	-8
MLF			<±1			155	-2	-6	-6	-9

Neural		*R. lateral bend (90°)*					*R. oblique ext (135°)*					*Extension (180°)*			
control	*t* (ms)	**C7**	**C4**	**C2**	**H**	*t* (ms)	**C7**	**C4**	**C2**	**H**	*t* (ms)	**C7**	**C4**	**C2**	**H**
X-rot															
KMLF	196	5	15	18	18	187	3	10	11	13			<±1		
KF	214	8	25	29	20	202	5	15	18	16			<±1		
MLF	195	5	15	18	19	185	2	8	12	15			<±1		
Y-rot															
KMLF	93	2	2	0	-2	199	4	-11	-24	-13	244	5	-14	-35	-25
KF	300	8	15	11	-4	216	5	-16	-33	-14	259	6	-22	-54	-30
MLF	287	2	-2	-7	-8	226	-1	-12	-18	-13	230	-4	-21	-28	-22
Z-rot															
KMLF	171	-4	-9	-11	-18	170	-3	-7	-9	-14			<±1		
KF	207	-2	-9	-12	-17	195	-1	-7	-11	-11			<±1		
MLF	157	-3	-9	-11	-17	167	-2	-8	-10	-15			<±1		

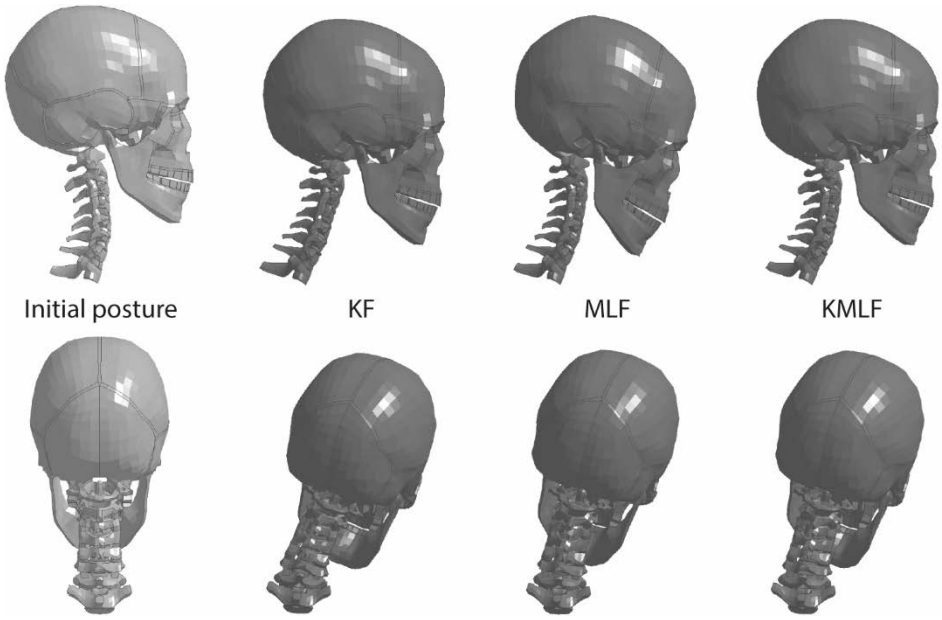

Fig. 6. Spinal curvature at time zero (initial posture) and 200 ms in two of the simulated conditions, i) and iii), causing neck flexion (0°, top row) and lateral bending (90°, bottom row) for the model with KF, MLF, and KMLF (from left to right).

IV. DISCUSSION

In this study, we implemented a reflex recruitment model to simulate head-neck responses in HBMs intended for automotive safety applications. Simulation of multidirectional low-g loading indicated that a combination of kinematics and muscle length feedback resulted in the largest overall reduction of head and vertebral displacements and rotations.

The current modelling approach included several assumptions in the implementation of two control paths based on inputs related to the vestibular system (KF) and muscle spindles (MLF). The model assumed a linear combination of KF and MLF excitation signals, adopted from analytical models [37–39]. Although this simplification may be representative in many situations the interaction of vestibular and muscle spindle reflexes is highly complex, it is likely context dependent and the relative contribution of each reflex modulated by the CNS for a specific action [39]. On the basis of previous work [2,22–26] the model used the head-neck vector to estimate vestibular feedback signals of head angular velocity, but alternative formulations could be considered. Linear acceleration and angular velocity of the head could be used as separate model inputs, based on anatomical and physiological considerations of the vestibular organ [40]. In addition, detailed models of vestibular sensory dynamics could be included, similar to [28]. We chose to have low complexity and this study did not attempt to model the actual activity of the CNS. Rather, the goal was to develop a modelling approach that could incorporate both of these types of feedback to explore how the feedback loops, in particular MLF influenced model responses in order to guide future modelling efforts for advancing HBM intended for development and evaluation of safety restraint systems. Future studies may investigate the potential benefit of implementing more sophisticated models of the CNS in HBMs for traffic safety applications.

MLF reduced vertebral rotations in all loading directions. MLF, similar to proprioceptive information, was the only direct source of information about internal neck kinematics, enabling adjustments by muscles inserting on the spine to maintain spinal curvature. Spinal alignment and intervertebral kinematics prior to and during impact have been suggested to play a role in neck injury mechanisms and outcome [31,41–44]. It is thus important that HBMs predict spinal kinematics during pre-crash to ensure the initial conditions before the crash are representative. Gathering detailed data on intervertebral kinematics from human subjects during dynamic events is difficult, which challenges thorough model validation. Although our study does not validate that MLF improves intervertebral kinematics prediction, it demonstrates the influence of including MLF in comparison to KF alone which is a common approach applied with current HBMs developed for pre-crash [2,22–26].

A load sharing definition was needed to transform a single control signal generated from kinematics feedback (KF) to a set of activation patterns determining the distribution of muscle activity in various loading directions

(Equation 1). Experimental neck muscle spatial tuning curves derived from multidirectional perturbations were used to define load sharing weight functions ($w_i(\alpha)$). As experimental data was only available for eight neck muscles, remaining muscles were grouped to share the same weights (Table I). The groups were defined based on presumed muscle function as described by anatomical texts and further guided by simulations where single muscles were activated and the resulting head kinematics monitored. Despite this simplification KF resulted in reduced head displacements in all loading directions. However, additional studies are needed to assess the influence of this simplification on the kinematic and muscle responses or to provide the spatial tuning curves for the remaining muscles. Gathering EMG data from individual neck muscles in dynamic conditions is challenging. Using data collected from isometric neck exertions may present an alternative approach to generate spatial tuning curves for the muscles in our model for which no experimental data was available. An isometric analysis that defined load sharing during simulated maximum voluntary contractions was presented in [45] and used in simulations of anterior–posterior oscillations [28]. However, qualitative comparison of spatial tuning curves from isometric contractions [46] to dynamic spatial tuning curves [30] indicated that, for some neck muscles, isometric spatial tuning is less focused. Isometrically derived synergies would potentially therefore be less suitable for dynamic omnidirectional predictions as they might result in overestimation of the contribution of some muscles in some loading directions. Future simulation studies that compare the influence of using spatial tuning curves from dynamic vs. isometric conditions on head-neck kinematics may shed further light on the applicability of using isometric data in dynamic simulations to guide where to focus experimental efforts.

The directional tuning of muscle activity, that is, the shape of the spatial tuning patterns, with KMLF was similar to KF for most muscles. Trap had more spread in activity, induced by MLF. This may be explained by the location of the points of insertion and origin of the muscle elements, ranging from the occipital bone to the lateral end of the clavicle, resulting in excessive lengthening in some loading directions. STH activity was high in six out of eight directions. The high activity during flexion and lateral bending does not match experimental data or what can be presumed from the anatomical location of this muscle given its anterior position to the spinal column and relatively small leverage to generate counteracting extension or lateral bending moments. The high activity was a result of the lengthening of the superior STH elements as the mandible moved relative to a rigid beam representing the hyoid bone and onto which the element was attached (see Appendix for a more detailed description). For instance, during flexion (0° loading direction in Figs. 4 and 5) an initial protraction of the head initiated lengthening of this superior element. It is unclear if the muscles above the hyoid bone would have a spatial tuning similar to that depicted in Fig. 5 but the high activation levels in multiple directions seem unlikely. Previous research has pointed out the importance of including the hyoid muscles in neck models. Their relatively large moment arm allow them to contribute largely to the total flexion moment of the neck and they activate during induced head extension [12,30,47,48]. In our model the hyoid muscles were needed to counteract excessive extension of the upper cervical spine. However, it is possible a more detailed model of the hyoid bone and suprahyoid muscles would provide a more representative response.

The response of the HBM with the reflex recruitment model (KMLF) was evaluated for 1 g loading and compared to the passive model and implementation of each of the two reflex loops (KF and MLF). Other neck models with neural control, developed for automotive safety applications, have been applied in longitudinal loading [24,27] or as a part of whole body simulations [2,21,23,26], limiting meaningful comparisons to our model. A defined set of baseline simulation cases producing an isolated head-neck response would be beneficial to compare and validate head-neck models with neural control. Head falls, similar to the conditions simulated here, provide a simple setup that produces measureable head kinematics with accelerations level representative of pre-crash scenarios. A benefit of such a setup is the feasibility to perform an equivalent volunteer experiment (for multiple loading directions). This has been done for supine head falls producing neck extension in volunteers [27,49]. However, neither study included a sufficient description of the experimental setup, in particular regarding initial and boundary conditions, needed to perform a thorough comparison to model responses. We encourage further volunteer experiments with head falls in multiple directions, with well-defined inferior boundary conditions, that measure EMG and kinematics, to provide a set of omnidirectional data for segmental validation and model comparisons.

The results clearly indicate the potential of the KMLF to reduce head displacement and maintain head angle while avoiding non-physiological vertebral rotations, in multiple loading directions. The predictions from the model should be validated in future work. Applying the presented method for reflex recruitment the model was

capable of counteracting induced head motion in multiple directions, but should be evaluated using acceleration magnitudes and durations typical of real world pre-crash manoeuvers. The current model has the implicit objective of maintaining the head and neck in the original posture and was tested in unidirectional loading, but it is not yet clear whether the reflex recruitment model is capable of fully compensating for any particular time course of inertial loading. The model kinematic responses should be compared to experimental data from human subjects in replicated pre-crash vehicle manoeuvers such as emergency braking and steering. Further work to validate the muscle responses in realistic scenarios and asses the validity of using perturbation data for determining load sharing at other acceleration levels is also needed. Monitoring muscle activity in human subjects is methodologically challenging, but accurate muscle recruitment simulation is needed if the focus of the simulation is on forces, strains, and injury prediction in the neck.

V. CONCLUSIONS

This study implemented a neural control scheme for regulating neck muscle activity in a finite element occupant HBM. The results demonstrated that combining sensory information about head kinematics and individual muscle length to generate activation levels for each muscle resulted in the largest overall reduction of head and vertebral displacements and rotations in 1 g loading conditions. Including muscle length feedback enabled adjustments of spinal alignment which may improve the prediction of vertebral kinematics in some loading directions. Data on spinal kinematics of human subjects exposed to external loading are needed to verify these observations.

VI. ACKNOWLEDGEMENT

The work presented in this paper was carried out at SAFER, the Vehicle and Traffic Safety Centre, at Chalmers, Gothenburg, Sweden. It was funded by FFI (Strategic Vehicle Research and Innovation) by VINNOVA, the Swedish Transport Administration, the Swedish Energy Agency and by the industrial partners; Autoliv Research AB, and Volvo Car Corporation. The simulations were performed on resources at Chalmers Centre for Computational Science and Engineering (C3SE) provided by the Swedish National Infrastructure for Computing (SNIC).

VII. REFERENCES

[1] Wang Y, Bai Z, Fischer K, Adler A, Reed MP, Cao L, et al. A simulation study on the efficacy of advanced belt restraints to mitigate the effects of obesity for rear-seat occupant protection in frontal crashes. Traffic Inj Prev. 2015;16: S75–S83.

[2] Östh J, Brolin K, Bråse D. A human body model with active muscles for simulation of pre-tensioned restraints in autonomous braking interventions. Traffic Inj Prev. 2015;16: 304–313.

[3] Bose D, Crandall JR, Untaroiu CD, Maslen EH. Influence of pre-collision occupant parameters on injury outcome in a frontal collision. Accid Anal Prev. 2010;42: 1398–1407.

[4] Antona J, Ejima S, Zama Y. Influence of the driver conditions on the injury outcome in front impact collisions. Int J Automot Eng. 2011;2: 33–38.

[5] Guleyupoglu B, Schap J, Kusano KD, Gayzik FS. The effect of precrash velocity reduction on occupant response using a human body finite element model. Traffic Inj Prev. 2017;18: 508–514.

[6] de Jager M, Sauren A, Thunnissen J, Wismans J. A global and a detailed mathematical model fo head-neck dynamics. Stapp Car Crash J. 1996; 40: 269–281.

[7] Wittek A, Kajzer J, Haug E. Hill-type muscle model for analysis of mechanical effect of muscle tension on the human body response in a car collision using an explicit finite element code. JSME Int J. 2000;43 8–18.

[8] van der Horst MJ. Human head neck response in frontal, lateral and rear end impact loading - modelling and validation. Eindhoven University of Technology; Eindhoven, The Netherlands. 2002.

[9] Brolin K, Halldin P, Leijonhufvud I. The effect of muscle activation on neck response. Traffic Inj Prev. 2005;6: 67–76.

[10] Stemper BD, Yoganandan N, Cusick JF, Pintar FA. Stabilizing effect of precontracted neck musculature in whiplash. Spine. 2006;31: E733-8.

[11] Fice JB, Cronin DS. Investigation of whiplash injuries in the upper cervical spine using a detailed neck

model. J Biomech. 2012;45: 1098–1102.
[12] Chancey VC, Nightingale RW, Van Ee CA, Knaub KE, Myers BS. Improved Estimation of Human Neck Tensile Tolerance: Reducing the Range of Reported Tolerance Using Anthropometrically Correct Muscles and Optimized Physiologic Initial Conditions. Stapp Car Crash J. 2003;47: 135–153.
[13] Brolin K, Hedenstierna S, Halldin P, Bass C, Alem N. The importance of muscle tension on the outcome of impacts with a major vertical component. Int J Crashworthiness. 2008;13: 487–498.
[14] Dibb AT, Cox CA, Nightingale RW, Luck JF, Cutcliffe HC, Myers BS, Arbogast KB, Seacrist T, Bass CR. Importance of muscle activations for biofidelic pediatric neck response in computational models. Traffic Inj Prev. 2013;14: S116-27.
[15] Mortensen J, Trkov M, Merryweather A. Exploring novel objective functions for simulating muscle coactivation in the neck. J Biomech. 2018;11: 127-134.
[16] Behr M, Arnoux P-J, Serre T, Thollon L, Brunet C. Tonic Finite Element Model of the Lower Limb. J Biomech Eng. 2006;128: 223–228.
[17] Sugiyama T, Kimpara H, Iwamoto M, Yamada D. Effects of muscle tense on impact responses of lower extremity. Proceedings of the IRCOBI conference; 2007; Maastricht, The Netherlands. pp. 127–140.
[18] Chang C, Rupp JD, Kikuchi N, Schneider LW. Development of a Finite Element Model to Study the Effects of Muscle Forces on Knee-Thigh-Hip Injuries in Frontal Crashes Noboru Kikuchi. Stapp Car Crash J. 2008;52: 475–504.
[19] Chang C, Rupp JD, Reed MP, Hughes RE, Schneider LW. Predicting the Effects of Muscle Activation on Knee, Thigh, and Hip Injuries in Frontal Crashes Using a Finite-Element Model with Muscle Forces from Subject Testing and Musculoskeletal Modeling. Stapp Car Crash J. 2009;53: 291–328.
[20] Iwamoto M, Nakahira Y. A Preliminary Study to Investigate Muscular Effects for Pedestrian Kinematics and Injuries Using Active THUMS. Proceedings of the IRCOBI conference; 2014; Berlin, Germany. pp. 444–460.
[21] Meijer R, van Hassel E, Broos J, Elrofai H, van Rooij L, van Hooijdonk P. Development of a Multi-Body Human Model that Predicts Active and Passive Human Behaviour. Proceedings of the IRCOBI conference; 2012; Ireland. pp. 622–636.
[22] Meijer R, Broos J, Elrofai H, de Bruijn E, Forbes P, Happee R. Modelling of bracing in a multi-body active human model. Proceedings of the IRCOBI conference, 2013; Gothenburg, Sweden. pp. 576–587.
[23] Östh J, Eliasson E, Happee R, Brolin K. A method to model anticipatory postural control in driver braking events. Gait Posture. 2014;40: 664–669.
[24] Nemirovsky N, van Rooij L. A new methodology for biofidelic head-neck postural control. Proceedings of the IRCOBI conference; 2010; Hanover, Germany. p. 71–84.
[25] Östh J, Brolin K, Carlsson S, Wismans J, Davidsson J. The occupant response to autonomous braking: a modeling approach that accounts for active musculature. Traffic Inj Prev. 2012;13: 265–77.
[26] Iwamoto M, Nakahira Y. Development and validation of the Total HUman Model for Safety (THUMS) version 5 containing multiple 1D muscles for estimating occupant motions with muscle activation during side impacts. Stapp Car Crash J. 2015;59: 53–90.
[27] Feller L, Kleinbach C, Fehr J, Schmitt S. Incorporating Muscle Activation Dynamics into the Global Human Body Model. Proceedings of the IRCOBI conference; 2016; Malaga, Spain. p. 512–523.
[28] Happee R, de Bruijn E, Forbes PA, van der Helm FCT. Dynamic head-neck stabilization and modulation with perturbation bandwidth investigated using a multisegment neuromuscular model. J Biomech. 2017;58: 203–211.
[29] Brolin K, Stockman I, Subramanian H, Gras L-L, Östh J. Development of an Active 6-Year-Old Child Human Body Model for Simulation of Emergency Events. Proceedings of the IRCOBI conference; 2015; Lyon, France. pp. 689–700.
[30] Ólafsdóttir JM, Brolin K, Blouin J-S, Siegmund GP. Dynamic spatial tuning of cervical muscle reflexes to multidirectional seated perturbations. Spine. 2015;40: E211-9.
[31] Östh J, Mendoza-Vazquez M, Sato F, Svensson MY, Linder A, Brolin K. A female head–neck model for rear impact simulations. J Biomech. 2017;51: 49–56.
[32] Todd NPM, McLean A, Paillard A, Kluk K, Colebatch JG. Vestibular evoked potentials (VsEPs) of cortical origin produced by impulsive acceleration applied at the nasion. Exp Brain Res. 2014;232: 3771–3784.
[33] der Helm FCT, Rozendaal LA. Musculoskeletal systems with intrinsic and proprioceptive feedback. In: Winters JM, Crago PE, editors. Biomechanics and neural Control of posture and movement. New York: Springer; 2000. p. 164–174.
[34] Macefield G, Gandevia S. Peripheral and central delays in the cortical projections from human truncal

muscles. Brain. 1992;115: 123–135.
[35] Winters JM, Stark L. Analysis of Fundamental Human Movement Patterns Through the Use of In-Depth Antagonistic Muscle Models. IEEE Trans Biomed Eng. 1985; 826–839.
[36] Ólafsdóttir JM, Östh JKH, Davidsson J, Brolin KB. Passenger kinematics and muscle responses in autonomous braking events with standard and reversible pre-tensioned restraints. Proceedings of the IRCOBI conference; 2013; Gothenburg, Sweden. p. 602–617.
[37] Peng GCY, Hain TC, Peterson BW. Predicting vestibular, proprioceptive, and biomechanical control strategies in normal and pathological head movements. IEEE Trans Biomed Eng. 1999;46: 1269–1680.
[38] Peterson W. Current approaches and future directions to understanding control of head movement. Prog Brain Res. 2004;143: 367–381.
[39] Forbes P. Sensorimotor control of the head neck system. Delft University of Technology; Delft, The Netherlands. 2014.
[40] Angelaki DE, Cullen KE. Vestibular System: The Many Facets of a Multimodal Sense. Annu Rev Neurosci. 2008;31: 125–150.
[41] Yoganandan N, Pintar FA, Gennarelli TA, Eppinger RH, Voo LM. Geometrical effects on the mechanism of cervical spine injury due to head impact. Proceedings of the IRCOBI conference; 1999; Sitges, Spain. p. 261–270.
[42] Stemper BD, Yoganandan N, Pintar FA. Effects of abnormal posture on capsular ligament elongations in a computational model subjected to whiplash loading. J Biomech. 2005;38: 1313–1323.
[43] Siegmund GP, Winkelstein B a, Ivancic PC, Svensson MY, Vasavada A. The anatomy and biomechanics of acute and chronic whiplash injury. Traffic Inj Prev. 2009;10: 101–112.
[44] Sato F, Odani M, Miyazaki Y, Yamazaki K, Osth J, Svensson M. Effects of whole spine alignment patterns on neck responses in rear end impact. Traffic Inj Prev. 2016;18: 199–206.
[45] de Bruijn E, van der Helm FCT, Happee R. Analysis of isometric cervical strength with a nonlinear musculoskeletal model with 48 degrees of freedom. Multibody Syst Dyn. 2015;36: 339–362.
[46] Siegmund GP, Blouin J-S, Brault JR, Hedenstierna S, Inglis JT. Electromyography of superficial and deep neck muscles during isometric, voluntary, and reflex contractions. J Biomech Eng. 2007;129: 66–77.
[47] Oi N, Pandy MG, Myers BS, Nightingale RW, Chancey VC. Variation of neck muscle strength along the human cervical spine. Stapp Car Crash J. 2004;48: 397–417.
[48] Zheng L, Jahn J, Vasavada AN. Sagittal plane kinematics of the adult hyoid bone. J Biomech. Elsevier; 2012;45: 531–6.
[49] Ito Y, Corna S, Von Brevern M, Bronstein A, Gresty M. The functional effectiveness of neck muscle reflexes for head-righting in response to sudden fall. Exp Brain Res. 1997;117: 266–272.

VIII. APPENDIX

Modelled muscles

The neck muscles were modelled with 188 one-dimensional Hill-type elements according to Table AI. The THUMS model does not include a hyoid bone. The hyoid muscles, which insert on the hyoid bone were therefore modelled with insertion on the mandible, albeit rerouted at a rigid beam at the approximate hyoid position relative to the spinal column and constrained to C4. Each hyoid muscle element (part) thus had two elements in series (using LS-DYNA card *PART_AVERAGED), both of which got the same activation level, where the superior element approximated a suprahyoid muscle.

According to anatomical texts [1] the hyoid bone and the larynx (attached to the hyoid bone) can span the C3-C6 level in males. Data from Valenzuela et al. [2] suggests that on average the most superior and anterior point of the body of the hyoid is lower than the most inferior and anterior point on the body of C3 (see measurement H to H' for normal head posture in Table 1 in Valenzuela et al. [2]. Based on this information, the location of the "hyoid beam" was approximated to be at the C4 level.

TABLE AI
PHYSIOLOGICAL CROSS-SECTIONAL AREA (PCSA), ORIGIN AND INSERTION POINT, AND NUMBER OF ELEMENTS OF THE MUSCLES INCLUDED IN THE MODEL (SINGLE SIDE). ADAPTED FROM ÖSTH ET AL. [3]. REFER TO TABLE II IN [3] FOR RESPECTIVE REFERENCE ON PCSA, ORIGIN AND INSERTION.

Muscle name	No. Elements	PCSA [mm^2]	Origin	Insertion
Erector spinae longissimus cervicis	5	149	T. proc. C2–C6	T. proc. T2–T6
Erector spinae longissimus capitis	8	98	Mastoid process	T. proc. C4–T4
Erector spinae iliocostalis cervicis	3	99	P. tub. C4–C6	4th–6th rib
Multifidus cervicis	12	450	S. proc. C2–C7	T. proc. C5–T4
Semispinalis cervicis	4	310	S. proc. C2–C5	T. proc. T1–T4
Semispinalis thoracis	2	140	S. proc. C6–C7	T. proc. T5–T6
Semispinalis capitis	5	550	Occipital bone	S.A. proc. C4–C7, T. proc. T3
Splenius cervicis	3	144	T. proc. C1–C3	S. proc. T3–T5
Splenius capitis	6	312	Mastoid process	S. proc. C5–T3
Trapezius	3	378	Skull	Clavicula
Levator scapulae	4	312	T. proc. C1–C4	Scapula
Rectus capitis posterior minor	1	92	Occipital bone	P. tub. C1
Rectus capitis posterior major	1	168	Occipital bone	Spine of C2
Rectus capitis anterior	1	70	Skull	C1
Rectus capitis lateralis	1	70	Skull	C1
Obliqus capitis superior	1	88	Occipital bone	T. proc. C1
Obliqus capitis inferior	1	195	T. proc. C1	S. proc. C2
Scalenus posterior	3	105	T. proc. C4–C6	1st rib
Scalenus medius	6	138	C2–C7	1st rib
Scalenus anterior	4	188	A. tub. C3–C6	1st rib
Longus colli superior oblique	3	81	Anterior arch C1	T. proc. C3–C5
Longus colli vertical	4	90	Vertebral body C2–C4	Vertebral body C7–T3
Longus colli inferior oblique	2	40	T. proc. C5–C6	Vertebral body T1–T2
Longus capitis	4	136	Occipital bone	T. proc. C3–C6
Omohyoid	3 (1)	44*	Scapula	Hyoid bone
Sternohyoid	4 (2)	26*	Sternum	Hyoid bone
Sternothyroid	4 (2)	32*	Sternum	Hyoid bone
Sternocleidomastoid	2	492	Mastoid process	Clavicula and sternum

A. tub. = Anterior tubercle; P. tub. = Posterior tubercle; S. A. proc. = Superior articular process; T. proc. = Transverse process. Numbers within parenthesis represent the number of parts (*PART_AVERAGED).
*Borst et al. [4].

Strength Verification

The HBM's maximum isometric neck strength was evaluated in three simulations for flexion, extension and right lateral bending. Muscle elements associated with each of the three motions were maximally activated ($u_j = 1$) while the head was constrained by a beam element attached to the head opposite to the respective motion. Antagonist muscles were not activated. The cervical vertebra and skull were merged into a single rigid body during these simulations to avoid non-physiological intervertebral motions. Moreover, to verify the strength balance of the defined muscle synergies in flexion-extension, this setup was simulated with $u_j = w_i(\alpha)$ and $\alpha = 180°$ for flexion, $\alpha = 0°$ for extension (antagonists not active). The exerted head forces were extracted and the resulting moments at the C7-T1 level (resolved to the midpoint between the C7 process and the sternal notch) were compared to C7-T1 moments of male subjects reported in [6–9].

The maximum isometric neck strength of the model was above average volunteer strength in all directions, except for extension in one study (Table AII). It was however, within the standard deviation of Jordan et al. [7] and Fice et al. [9] for flexion and Jordan et al. [7], Vasavada et al. [8], and Fice et al. [9] for extension. The resulting C7-T1 moments, when muscles were activated according to the synergies defined by $w_i(\alpha)$, were 24.4 and 23.4 Nm for flexion and extension, respectively.

TABLE AII
COMPARISON OF MODEL ISOMETRIC NECK STRENGTH TO MALE VOLUNTEERS REPORTED IN MOMENTS ABOUT C7-T1. VALUES REPRESENT AVERAGE ± STANDARD DEVIATION IN NM.

	Nr. of subjects	Flexion	Extension	Lateral bending
Cagnie et al. [6]	48	24 ± 6	36 ± 8	
Jordan et al. [7]	50	30 ± 9	55 ± 14	
Vasavada et al. [8]	11	30 ± 5	52 ± 11	36 ± 8
Fice et al. [9]	9	30 ± 6	51 ± 11	32 ± 9
Model		35.7	54.8	44.9

The model's isometric neck strength in flexion and extension compared well to measures of a total of 70 male volunteers reported in three studies [7–9], but was generally above the average reported strength. The model's strength in lateral bending was above the reported standard deviation of 20 volunteers. The higher strength of the model was probably because the agonist muscles to each exertion were given an activation level of 100%. However, it is unlikely that the corresponding muscles were all recruited to their physiological maximum in the volunteers. For instance, trapezius and levator scapulae are mainly shoulder muscles and unlikely to exhibit a maximum contraction during voluntary neck extension [10]. EMG recordings during maximum voluntary contractions (MVCs) have shown that semispinalis capitis, semispinalis cervicis, trapezius, sternocleidomastoid, and sternohyoid muscles, generally do not contract maximally during lateral bending [11,12]. Applying maximum activation in the model might therefore explain the consistently higher moments than seen in the average male volunteer.

Verification of spatial tuning of muscle recruitment

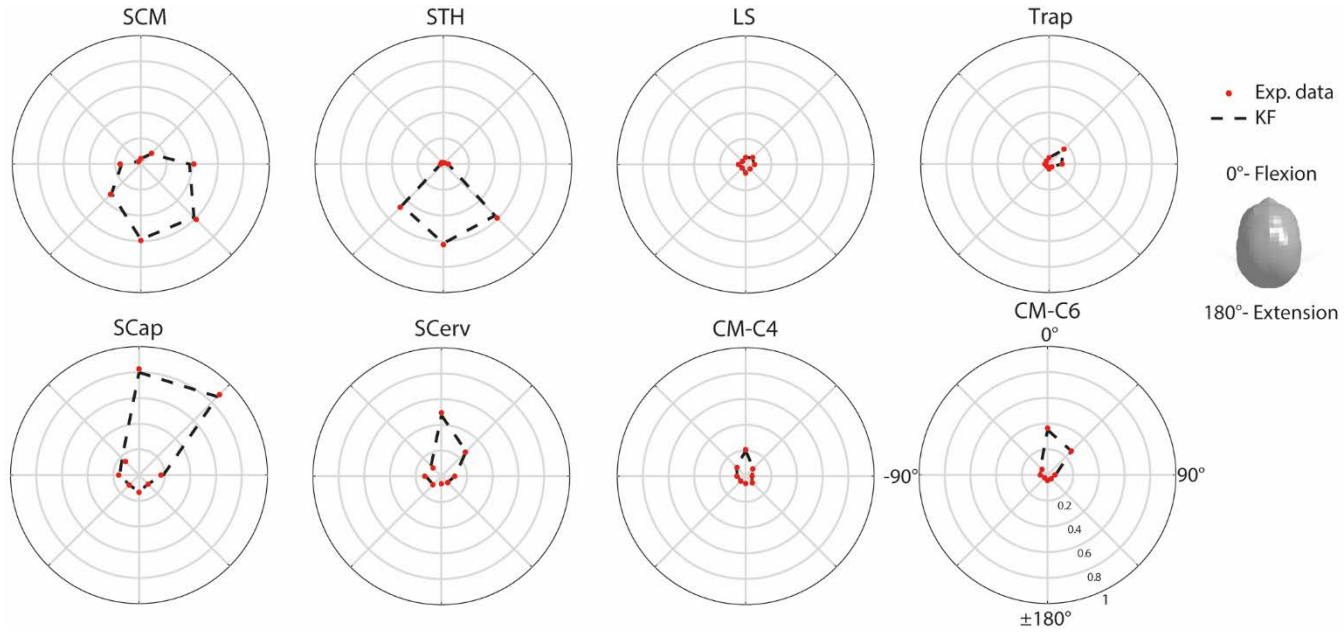

Fig. A1. Spatial tuning patterns with kinematics feedback (KF, dotted curves) compared to the implemented experimental spatial tuning curves (red dots) from Ólafsdóttir et al. [5] that were used to define load sharing between various muscle groups (weighting functions, $w_i(\alpha)$). All tuning curves show left muscle activation levels at 110 ms after loading onset. The '1' on the perimeter represents 100% activity.

References

[1] Standring S, editor. Gray's Anatomy – The anatomical basis of clinical practice. London, UK: Elsevier Churchill Livingstone; 2008.

[2] Valenzuela S, Miralles R, Ravera MJ, Zúñiga C, Santander H, Ferrer M, et al. Does head posture have a significant effect on the hyoid bone position and sternocleidomastoid electromyographic activity in young adults? Cranio. 2005;23: 204–211.

[3] Östh J, Brolin K, Carlsson S, Wismans J, Davidsson J. The occupant response to autonomous braking: a modeling approach that accounts for active musculature. Traffic Inj Prev. 2012;13: 265–77.
[4] Borst J, Forbes P a, Happee R, Veeger DHEJ. Muscle parameters for musculoskeletal modelling of the human neck. Clin Biomech. 2011;26: 343–51.
[5] Ólafsdóttir JM, Brolin K, Blouin J-S, Siegmund GP. Dynamic spatial tuning of cervical muscle reflexes to multidirectional seated perturbations. Spine. 2015;40: E211-9.
[6] Cagnie B, Cools A, De Loose V, Cambier D, Danneels L. Differences in Isometric Neck Muscle Strength Between Healthy Controls and Women With Chronic Neck Pain: The Use of a Reliable Measurement. Arch Phys Med Rehabil. 2007;88: 1441–1445.
[7] Jordan A, Mehlsen J, Bulow MP, Ostergaard K, Danneskiold-Somsoe B. Maximal isometric strength of the cervical musculature in 100 healthy volunteers. Spine. 1999;24: 1343–1348.
[8] Vasavada AN, Li S, Delp SL. Three-Dimensional Isometric Strength of Neck Muscles in Humans. Spine. 2001;26: 1904–1909.
[9] Fice JB, Siegmund GP, Blouin JS. Prediction of three dimensional maximum isometric neck strength. Ann Biomed Eng. 2014;42: 1846–1852. doi:10.1007/s10439-014-1046-0
[10] Moroney SP, Schultz AB, Miller JAA. Analysis and measurement of neck loads. J Orthop Res. 1988;6: 713–720.
[11] Gabriel D a, Matsumoto JY, Davis DH, Currier BL, An K-N. Multidirectional neck strength and electromyographic activity for normal controls. Clin Biomech. 2004;19: 653–8. doi:10.1016/j.clinbiomech.2004.04.016
[12] Siegmund GP, Blouin J-S, Brault JR, Hedenstierna S, Inglis JT. Electromyography of superficial and deep neck muscles during isometric, voluntary, and reflex contractions. J Biomech Eng. 2007;129: 66–77.